2024 IEEE/RSJ International Conference on Intelligent Robots and Systems (IROS)
October 14-18, 2024. Abu Dhabi, UAE

Integrated 3DOF Trajectory Tracking Control for Under-actuated Marine Surface Vehicles By Trajectory Linearization

Miguel Sempertegui[1] and J. Jim Zhu[2]

Abstract— **An integrated 3DOF trajectory tracking control algorithm with lateral drift correction for under-actuated Marine Surface Vehicles is presented using the Multi-Nested Loop Trajectory Linearization Control architecture. The sideslip angle is used as a virtual control effector for generating a lateral hydrodynamic force to correct the lateral drift due to a skid-turn, which is intrinsic to MSVs. The nominal sideslip angle is determined based on the kinematics and dynamics of the MSV along a nominal trajectory. Simulation results for a sub-scale vessel with significant vessel parameter perturbations are presented to demonstrate effectiveness of the proposed algorithm.**

I. INTRODUCTION

Path following and trajectory tracking are basic motion control tasks. The path following requires the vehicle to traverse a desired path constrained by vehicle kinematics with no consideration of acceleration and dynamic constraints. Whereas trajectory tracking deals with variable velocity along a desired path by generating the required force and moment, while regulating the tracking error. Path following is useful for path planning and guidance, while trajectory tracking is useful for precision agile maneuvers and navigation in congested waters. Both tasks require effective lateral control to reduce the cross-track error. Airplanes generate a lateral force by banking, wheeled ground vehicles rely on strong ground traction or banked roads to provide lateral force, and fully actuated Marine Surface Vehicles (MSVs) use independent lateral thrusters or propellers such as the ones in [1]–[7]. However, under-actuated MSVs can only make skid-turns, which may incur large cross-track errors due to drift. This intrinsic drift while turning behavior is a recognized challenge for the motion control of under-actuated MSV [8]–[10]. Nevertheless, one way to effect lateral control for this class of MSVs is to utilize the sideslip angle, which can induce a large hydrodynamic lateral force. This approach presents two challenges: (i) The required sideslip angle for control, which accounts for kinematics and dynamics along a nominal trajectory, needs to be determined and (ii) A method for utilizing the rudder to satisfy both lateral and directional control commands needs to be devised.

Additionally, since drift is caused by the coupling between the transnational and rotational motions of an MSV, an integrated motion controller is highly desirable. Furthermore, it has been recognized that the complexity "drastically increases if speed and heading are stabilized simultaneously"[9]. As a consequence, research results on this topic appear to be scarce in the literature. An integrated 3DOF controller was proposed in [11]. However, the resulting control law is very complex and unintuitive for performance synthesis and tuning, and the simulation results presented do not seem to be practical.

In this paper, an integrated 3DOF trajectory tracking control algorithm for under-actuated MSVs is presented using the Multi-Nested Loop (MNL) Trajectory Linearization Control (TLC) architecture. The lateral drift challenge is tackled by using the sideslip angle as a virtual control effector. A key enabling novel algorithm is proposed for computing the nominal sideslip angle that generates the required lateral hydrodynamic force to achieve precise skid-turns. The sideslip command uses the controlled directional subsystem as its actuator, and the conflict in lateral and rotational controls by a single rudder is resolved by time-scale separation, facilitated by the cascaded MNL structure. To the authors' best knowledge such approach is novel in the MSV field. Synthesis and tuning of the inverse dynamics in the open-loop nominal controller of the TLC is demonstrated by simulation. A well-tuned nominal controller trims the vehicle to the vicinity of the nominal trajectory, resulting in small nonlinear tracking errors for exponential stabilization by linearization, which significantly increases the validity of the linear approximation and domain of stability. The linear feedback controllers provide exponential stability, albeit local, for the closed-loop tracking error dynamics, which is well known to be robust to regular and singular perturbations [12]–[14]. The effectiveness of the proposed control algorithm is demonstrated by simulations on a well-known sub-scale vessel model for circular and sinusoidal trajectories starting at rest to show transient and steady state performances. Simulation results with perturbations to the moment of inertia value in the vehicle and controller are also presented, showing minimal performance degradation.

The proposed nominal sideslip algorithm for tracking control extends the results in [9], [10], [15] for path following to the trajectory tracking problem, while eliminating the restriction on small and slowly varying sideslip angles. The overall MNL-TLC algorithm extends the works presented in [16]–[20] for MSV motion control using TLC, while adding a novel lateral control actuation using sideslip angle. Compared to the integrated 3DOF MSV tracking controllers in [11], [21], the proposed open-loop and closed-loop controllers are not only simpler, but also more physically intuitive in synthesis and tuning of the controller parameters.

[1]Miguel Sempertegui is a Ph.D. student of Electrical Engineering and Computer Science, Russ College of Engineering, Ohio University, Athens, OH 45701, USA ms070613@ohio.edu

[2]J. Jim Zhu Ph.D. is with Faculty of Russ College of Engineering, Ohio University, Athens, OH 45701, USA zhuj@ohio.edu

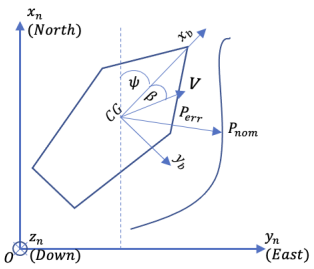

Fig. 1. MSV Coordinate Reference Frames

It also provides more robust exponential stability without resorting to piece-wise-arc trajectories.

This paper is organized as follows. Vehicle modeling is presented in Section II. Section III discuses the design of the open-loop nominal and closed-loop feedback controllers for each loop, and allocation of the force and moment commands to actuators. The simulation results are presented in Section IV. Section V concludes the paper with a summary of the main contributions and further research needed.

II. VEHICLE MODELING

The MSV kinematic and dynamic equations are determined relative to the navigation frame (n-frame) and the body-fixed frame (b-frame), shown in Fig. 1. The n-frame follows the North-East-Down (NED) convention. The b-frame is fixed to the Center of Gravity (CG) of the vessel with bow-starboard-down convention. A standard 3DOF MSV model as given in [22] is adopted with assumptions: 1) Flat and inertial Earth, 2) no rolling, heaving or pitching motions, 3) CG and center of buoyancy (CB) are co-located vertically on the z-axis, 4) *xz*-plane symmetry, 5) calm water and absence of wind.

While these simplifying assumptions may facilitate controller design, they require sufficient robustness from the controller. Some approaches [23]–[26] relay on the use of NN to estimate parametric perturbations and disturbances to achieve the needed robustness of the overall controller. In this paper, we rely on the the inherit robustness of the exponential stability by the proposed control algorithm.

A. Rigid-Body Model

Unlike the typical MSV model [22], the present work models the vessel as a cascade multi-loop system, where the translational kinematics, translational dynamics, rotational kinematics and rotational dynamics are given by:

$$\begin{bmatrix}\dot{x}\\ \dot{y}\end{bmatrix} = \begin{bmatrix}\cos(\psi) & -\sin(\psi)\\ \sin(\psi) & \cos(\psi)\end{bmatrix}\begin{bmatrix}u\\ v\end{bmatrix} \tag{1}$$

$$\begin{bmatrix}\dot{u}\\ \dot{v}\end{bmatrix} = \begin{bmatrix}0 & r\\ -r & 0\end{bmatrix}\begin{bmatrix}u\\ v\end{bmatrix} + \frac{1}{m}F \tag{2}$$

$$\dot{\psi} = r \tag{3}$$

$$\dot{r} = \frac{1}{I_z}N \tag{4}$$

where m and I_z are the vehicle's mass and yaw moment of inertia, respectively.

B. Force and Moment Models

Unlike typical modeling approaches wherein the generalized force model is lumped with the rigid body model, the generalized forces are modeled separately in the MNL-TLC approach. The force vector in (2) is given by [22]:

$$F = \begin{bmatrix}F_x\\ F_y\end{bmatrix} = F_H + F_D + F_C + F_W \tag{5}$$

where F_H and F_D are given by [22]:

$$F_H = \begin{bmatrix}X_{\dot{u}}\dot{u}\\ Y_{\dot{v}}\dot{v} + Y_{\dot{r}}\dot{r}\end{bmatrix} - \begin{bmatrix}Y_{\dot{v}}vr + Y_{\dot{r}}r^2\\ -X_{\dot{u}}ur\end{bmatrix} \tag{6}$$

$$F_D = \begin{bmatrix}X_u u + X_{|u|u}|u|u + X_{uuu}u^3\\ Y_v v + Y_r r + Y_{|v|v}|v|v + Y_{|r|v}|r|v + Y_{|v|r}|v|r + Y_{|r|r}|r|r\end{bmatrix} \tag{7}$$

F_C is the control force of the actuators, and F_w represent the disturbance forces due to wind, currents and waves.

The yaw moment in (4) is given by [22]:

$$N = N_{CR} + N_H + N_D + N_C + N_W \tag{8}$$

where N_{CR} is the moment due the the coriolis and centripetal effects, which is zero when the body-frame origin and CG are co-located, N_H and N_D moments are given by [22]:

$$N_H = Y_{\dot{r}}\dot{v} + N_{\dot{r}}\dot{r} + Y_{\dot{v}}uv - Y_{\dot{r}}ur - X_{\dot{u}}uv \tag{9}$$

$$N_D = N_v v + N_r r + N_{|v|v}|v|v + N_{|r|v}|r|v + N_{|v|r}|v|r + N_{|r|r}|r|r \tag{10}$$

N_C is the control moment produced by the actuators, and N_W is the disturbance due to wind, currents and waves. In eqs. (6), (7), (9), and (10), $X_{\dot{u}}, Y_{\dot{v}}$ and $N_{\dot{r}}$ are the added masses, and the remaining X_*, Y_* and N_* parameters are the hydrodynamic damping derivatives.

C. Actuator Model

1) Actuator Forces and Moment: Without loss of generality, a single propeller-rudder actuator set is considered, as shown in Fig. 2. The same control effect can be achieved by using a dual propeller-rudder system, which allows for yaw control by differential thrust. However, at cruising speeds, the yaw control effectiveness of differential thrust is negligible compared to that of the rudders. It is useful only for very low speed maneuvering, which is not the focus of the current paper. The hydrodynamic thrust $\mathcal{T}$, the drag $\mathcal{D}$ and transversal lift force $\mathcal{L}$ of the rudder are functions of the propeller shaft angular velocity ω_{sh} and the rudder angle δ_{rd}. These nonlinear coupled functions are given by [27]:

$$\mathcal{T}(\omega_{sh}, \delta_{rd}) = \begin{cases} k_{\mathcal{T}_p}{\omega_{sh}}^2 & \omega_{sh} \geq 0 \\ k_{\mathcal{T}_n}|\omega_{sh}|\omega_{sh} & \omega_{sh} < 0 \end{cases} \tag{11}$$

$$\mathcal{D}(\omega_{sh}, \delta_{rd}) = \begin{cases} \mathcal{T}(1 + k_{\mathcal{D}_n}\omega_{sh})(k_{\mathcal{D}\delta_1}|\delta_{rd}|) & \omega_{sh} \geq 0 \\ 0 & \omega_{sh} < 0 \end{cases} \tag{12}$$

$$\mathcal{L}(\omega_{sh}, \delta_{rd}) = \begin{cases} \mathcal{T}(1 + k_{\mathcal{L}_n}\omega_{sh})(k_{\mathcal{L}\delta_1})\delta_{rd} & \omega_{sh} \geq 0 \\ 0 & \omega_{sh} < 0 \end{cases} \tag{13}$$

where $k_{\mathcal{T}_p}$ and $k_{\mathcal{T}_n}$ are the thrust coefficients of the propeller for forward and reverse motion respectively, $k_{\mathcal{D}_n}$ and $k_{\mathcal{D}\delta_1}$

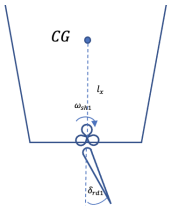

Fig. 2. MSV Propulsion System Configuration

are the drag coefficients of the rudder, $k_{\mathcal{L}_n}$ and $k_{\mathcal{L}\delta_1}$ are the lift coefficients of the rudder. Equations (11)-(13) are given in the actuator reference frame parallel to the b-frame, whose origin is at $(l_x, 0)$ with respect to the origin of the b-frame. The resulting generalized force vector is given by:

$$\begin{bmatrix} F_{C,x} \\ F_{C,y} \\ N_C \end{bmatrix} = \begin{bmatrix} \mathcal{T} - \mathcal{D} \\ \mathcal{L} \\ \mathcal{L} l_x \end{bmatrix} \tag{14}$$

2) Actuator Dynamics Model: For simplicity, the propeller and rudder actuators are modeled as second order transfer functions of the form:

$$G_{sh}(s) = \frac{\omega_{n,sh}^2}{s^2 + 2\zeta_{sh}\omega_{n,sh}s + \omega_{n,sh}^2} \tag{15}$$

$$G_{rd}(s) = \frac{\omega_{n,rd}^2}{s^2 + 2\zeta_{rd}\omega_{n,rd}s + \omega_{n,rd}^2} \tag{16}$$

III. TLC CONTROLLER DESIGN

The TLC architecture is composed of two controllers: an open-loop nominal controller and a closed-loop feedback controller. The nominal controller is design and constructed via dynamic pseudo-inversion of the vehicle model. The feedback controller regulates the error dynamics and achieve exponential stability. A TLC based controller produces a tracking command u_{com} that is the sum of the nominal u_{nom} and the feedback control u_{ctrl} as seen in Fig. 3.

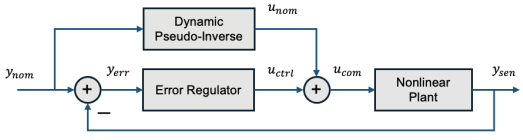

Fig. 3. Basic TLC Structure

The overall MSV controller design is simplified by the cascade 3DOF MSV into subsystems (1)-(4). This structure is denominated MNL-TLC. The basic TLC structure in Fig. 3 is applied to each subsystem. Exponential stability of the overall system is achieved one subsystem at a time by the time scale separation principle [12], [13]. This structure is denominated MNL-TLC as shown in Fig. 4. The control algorithm is realized under the assumptions:

Assumption 1: A feasible nominal pose trajectory $\eta_{nom}(t) = [x_{nom}(t), y_{nom}(t), \psi_{nom}(t)]^T$ is provided by an external trajectory planner, not covered in the current work. Due to the MNL partition, the translational position is represented as $P(t) = [x(t), y(t)]^T$ in the work below.

Assumption 2: The reference trajectory $\eta_{nom} \in C^2$.

Assumption 3: All motion states $\eta(t) = [x(t), y(t), \psi(t)]^T$ and $\nu(t) = [u(t), v(t), r(t)]^T$ are directly measurable.

A. Open- Loop Nominal Controller Design

1) Rigid-body Dynamic Inversion: By Assumption 2, the nominal controls are obtained via dynamic psuedo-inversion of the equations of motion (1)-(4):

$$V_{nom} = \begin{bmatrix} \cos(\psi_{nom}) & -\sin(\psi_{nom}) \\ \sin(\psi_{nom}) & \cos(\psi_{nom}) \end{bmatrix}^{-1} \dot{\hat{P}}_{nom} \tag{17}$$

$$\begin{bmatrix} F_{x,nom} \\ F_{y,nom} \end{bmatrix} = m \begin{bmatrix} \dot{\hat{u}}_{nom} \\ \dot{\hat{v}}_{nom} \end{bmatrix} - m \begin{bmatrix} 0 & r_{nom} \\ -r_{nom} & 0 \end{bmatrix} \begin{bmatrix} u_{nom} \\ v_{nom} \end{bmatrix} \tag{18}$$

$$\psi_{nom} = \chi_{ref} - \beta_{nom}{}^1 \tag{19}$$

$$r_{nom} = \dot{\hat{\psi}}_{nom} \tag{20}$$

$$N_{nom} = I_z \dot{\hat{r}}_{nom} \tag{21}$$

where $\hat{*}$ and $\dot{\hat{*}}$ denote a lowpass filtered variable $*$ and its derivative respectively, which are obtained using a pseudo-differentiator with state-space realization:

$$\begin{bmatrix} \dot{\hat{*}} \\ \ddot{\hat{*}} \end{bmatrix} = \begin{bmatrix} 0 & 1 \\ -\omega_{n,diff}{}^2 & -2\zeta_{diff}\omega_{n,diff} \end{bmatrix} \begin{bmatrix} \hat{*} \\ \dot{\hat{*}} \end{bmatrix} + \begin{bmatrix} 0 \\ \omega_{n,diff}{}^2 \end{bmatrix} * \tag{22}$$

The pseudo-differentiator is needed since exact derivative operation is anticausal, thus not realizable in real-time operations. Furthermore, it allows for a desired dynamics of the nominal motion variables to be designed by selecting the values of ζ_{diff} and $\omega_{n,diff}$.

2) Force and Moment Inversion: The longitudinal force and torque commanded to the actuators are calculated by inversion of Eqs. (5) and (8).

$$F_{Cx,com} = F_{x,nom} - F_{H,xnom} - F_{D,xnom} \tag{23}$$

$$N_{C,com} = N_{nom} - N_{H,nom} - N_{D,nom} \tag{24}$$

3) Lateral Force Generation: The lateral force F_y is controlled by the virtual control effector β_{nom} using the the directional loop as the actuator, where β_{nom} is computed from the reference pose trajectory $\eta_{nom}(t)$ as shown in Fig. 5.

Step 1: The required lateral force $F_{y,req}$ is calculated from the nominal trajectory η_{nom} by:

$$V_{ref} = \begin{bmatrix} \cos(\chi_{nom}(t)) & -\sin(\chi_{nom}(t)) \\ \sin(\chi_{nom}(t)) & \cos(\chi_{nom}(t)) \end{bmatrix}^{-1} \dot{\hat{P}}_{nom} \tag{25}$$

$$r_{ref} = \dot{\hat{\chi}}_{nom} \tag{26}$$

$$\begin{bmatrix} F_{x,req} \\ F_{y,req} \end{bmatrix} = m\dot{\hat{V}}_{ref} - m \begin{bmatrix} 0 & r_{ref} \\ -r_{ref} & 0 \end{bmatrix} V_{ref} \tag{27}$$

[1]Note that ψ and χ are sometimes referred as 'yaw' and 'heading' angles, respectively in the literature.

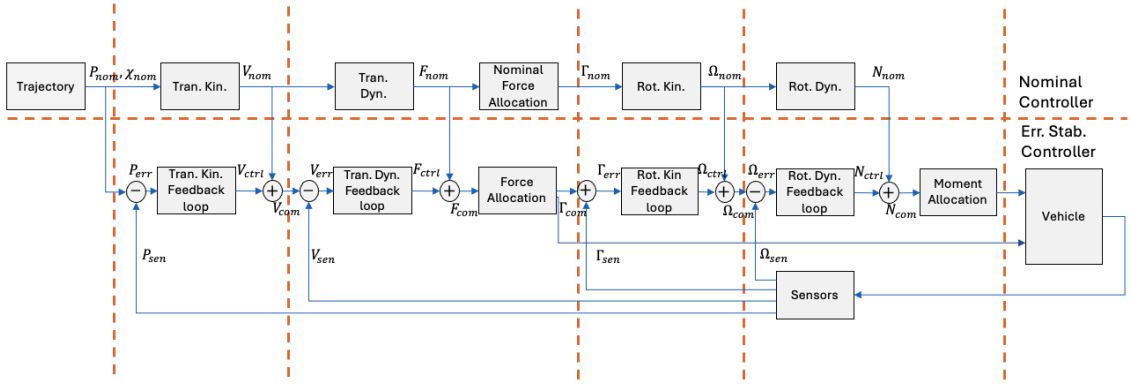

Fig. 4. TLC block diagram architecture

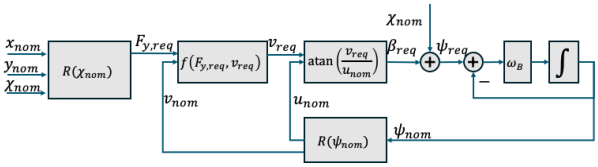

Fig. 5. Lateral Force Allocation

Step 2: The required lateral velocity v_{req} is approximated from $F_{y,req}$ with the most significant coefficients, $Y_{|v|v}$ and Y_v. Then, v_{req} is calculated by:

$$v_{req} = sign(v_{nom}) \left(\frac{-Y_v + \sqrt{Y_v^2 + p}}{2Y_{|v|v}} \right) \tag{28}$$

where:

$$p = \begin{cases} 4F_{y,req}Y_{|v|v}sign(v_{nom}) & sign(F_{y,req}) \neq sign(v_{nom}) \\ 0 & otherwise. \end{cases} \tag{29}$$

Eq. (28) presents the erroneous condition $sign(F_{y,req}) = sign(v_{nom})$ caused by approximation errors as $v_{nom} \to 0$.

Step 3: The required sideslip β_{req} is calculated using v_{req} from (28) and u_{nom} by the approximation:

$$\beta_{req}(t) = \frac{v_{req}(t)}{u_{nom}(t)} \tag{30}$$

Step 4: β_{req} is used to compute the required heading angle:

$$\psi_{req} = \chi_{nom} - \beta_{req} \tag{31}$$

Step 5: ψ_{req} is used to compute the rate of change:

$$\dot{\psi}_{nom}(t) = \omega_B \left(\psi_{req}(t) - \psi_{nom}(t) \right) \tag{32}$$

where ω_B is a design parameter.

Remark: The strict assumptions of constant β in [9], and the constant generalized velocities for a trajectory composed of straight lines and circular segments [21] are eliminated in the present approach, so long as the nominal trajectory is smooth according to Assumptions 1-2.

4) Synthesis and Tuning of the Inverse Dynamics: Although the MNL-TLC controller architecture has appeared in the literature for motion control of various types of vehicles, there has been little discussion regarding the tuning and performance of the inverse dynamics in the open loop controller. Since a better open loop performance leads to increased stability margins and less corrective actuator activities in the closed loop controller, its performance merits attention. While the static inverse determines the steady-state error of the nominal controller, the dynamics of the pseudo-differentiator (22) determines the transient performance.

In what follows, the effects of under-tuning, over-tuning, and proper tuning of the nominal controller are presented and discussed by simulation for the MSV controller. The tuning of the controller is done in such a way that the subsystem being tuned should have a fast enough response so as not to slowdown its outer loop motion, but not too fast as to demand excessive response from its inner loop. It is also noted that the translational kinematics need to have enough bandwidth to accommodate the highest expected frequency (maximum curvature and speed) in the desired translational motion. A good rule of thumb is to assign a $\omega_{n,diff}$ 10X of the expected motion bandwidth.

To exemplify the tuning process, Fig. 6 and Fig. 7 show the open-loop trajectory tracking and actuator signals of a sub-scale MSV model used in Section IV below for a circular trajectory starting at rest. For an under-tuned open-loop controller where the bandwidth $\omega_{n,diff}$ is too small, there is a lack of initial acceleration. This produces a large initial error which leads to a large deviation from the nominal trajectory. An over-tuned controller with a very high $\omega_{n,diff}$ produces a good initial acceleration and initial tracking. However, the actuators show excessively high rate of activities which may cause actuator wear-and-tear, or actuator saturation that leads to instability in closed-loop control. A well-tuned controller produces a good trade-off in both tracking performance and actuator signal demand. It is worth noting that the observed increasing position error is not due to instability. Rather, they are the cumulative errors from the initial transient response, which will be eliminated by the feedback controller. It is also noticed that the diameter of the steady-state circular orbits

are about 10% smaller than the nominal. This is the result of about 4% rudder allocation error, which can be compensated by the feedback controller.

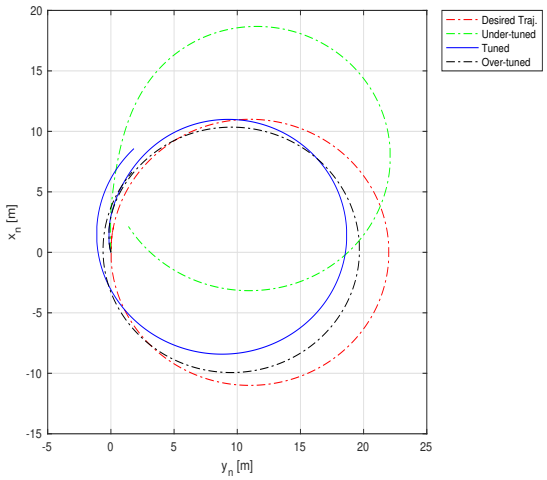

Fig. 6. Nominal Control Inertial Position Tracking

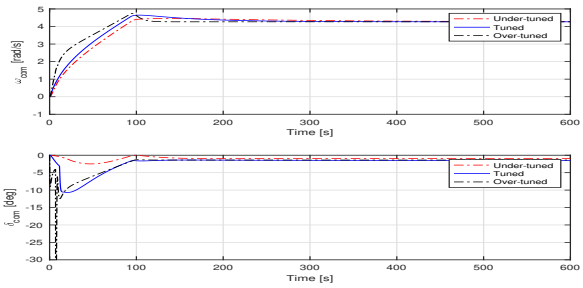

Fig. 7. Nominal Control Actuator Command Signals

B. Feedback Controller Design

The feedback controller is designed to exponentially stabilize the deviations of the sensed motion variables from their corresponding command trajectories. The tracking errors for each loop are defined as follows:

$$P_{err} = P_{sen} - P_{com} \tag{33}$$
$$V_{err} = V_{sen} - V_{com} \tag{34}$$
$$\psi_{err} = \psi_{sen} - \psi_{com} \tag{35}$$
$$r_{err} = r_{sen} - r_{com} \tag{36}$$

The error dynamics are then derived by taking the derivative of (34)-(36) which in general are nonlinear and time-varying. Assumption 3 allows for the direct computation of the error dynamics without the need for observers. Exponential stability is achieved with a LTV control law for the linearized tracking error dynamics by eigenvalue assignment. The feedback controllers are designed and tuned one loop at a time from the innermost loop, with all its inner loop dynamics neglected, provided that the closed-loop bandwidth ω_n is sufficiently small compared to its inner-loops. A detailed explanation of this process can be found in [28].

The n-frame position error P_{err} is mapped into the b-frame as the down-range vector R_b:

$$R_b = -\begin{bmatrix} \cos(\psi_{nom}) & -\sin(\psi_{nom}) \\ \sin(\psi_{nom}) & \cos(\psi_{nom}) \end{bmatrix}^{-1} P_{err} \tag{37}$$

Then, the linearized b-frame error dynamics are given by:

$$\dot{R}_b = \begin{bmatrix} 0 & r_{nom} \\ -r_{nom} & 0 \end{bmatrix} R_b + V_{ctrl} \tag{38}$$

$$\begin{bmatrix} \dot{u}_{err} \\ \dot{v}_{err} \end{bmatrix} = \begin{bmatrix} 0 & r_{nom} \\ -r_{nom} & 0 \end{bmatrix} \begin{bmatrix} u_{err} \\ v_{err} \end{bmatrix} + \frac{1}{m} \begin{bmatrix} F_{x,ctrl} \\ F_{y,ctrl} \end{bmatrix} \tag{39}$$
$$\dot{\psi}_{err} = r_{ctrl} \tag{40}$$
$$\dot{r}_{err} = \frac{1}{I_z} N_{ctrl} \tag{41}$$

The trajectory tracking error controls are designed as Proportional-Integral (PI) controllers such that they cancel the plant dynamics and assign the desired closed-loop dynamic response which can be time-varying. The designed control laws are as follows:

$$V_{ctrl} = -K_{P1} R_b - K_{I1} \int_0^t R_b d\tau \tag{42}$$

$$\begin{bmatrix} F_{x,ctrl} \\ F_{y,ctrl} \end{bmatrix} = -K_{P2} \begin{bmatrix} u_{err} \\ v_{err} \end{bmatrix} - K_{I2} \begin{bmatrix} \int_0^t u_{err} d\tau \\ \int_0^t v_{err} d\tau \end{bmatrix} \tag{43}$$

$$\psi_{ctrl} = \beta_{ctrl} = tan^{-1} \frac{v_{err}}{u_{nom}} \tag{44}$$
$$r_{ctrl} = -K_{P3} \psi_{err} - K_{I3} \int_0^t \psi_{err} d\tau \tag{45}$$
$$N_{ctrl} = -K_{P4} r_{err} - K_{I4} \int_0^t r_{err} d\tau \tag{46}$$

where:

$$K_{P1}(t) = \begin{bmatrix} a_{111}(t) & r_{nom} \\ -r_{nom} & a_{121}(t) \end{bmatrix} \quad K_{I1}(t) = \begin{bmatrix} a_{112}(t) & 0 \\ 0 & a_{122}(t) \end{bmatrix}$$
$$K_{P2}(t) = m \begin{bmatrix} a_{211}(t) & r_{nom} \\ -r_{nom} & a_{221}(t) \end{bmatrix} \quad K_{I2} = m \begin{bmatrix} a_{212}(t) & 0 \\ 0 & a_{222}(t) \end{bmatrix}$$
$$K_{P3}(t) = a_{311}(t) \quad K_{I3}(t) = a_{312}(t)$$
$$K_{P4}(t) = I_z a_{411}(t) \quad K_{I4}(t) = I_z a_{412}(t)$$

where:

$$a_{ij1}(t) = 2\zeta_{ij}\omega_{nij}(t) \tag{47}$$
$$a_{ij2}(t) = \omega_{nij}^2(t) - \frac{\dot{\omega}_{nij}(t)}{\omega_{nij}(t)} \tag{48}$$

The constant damping ratio ζ_{ij} and bandwidth time varying $\omega_{n,ij}(t)$ are used to synthesize the desired feedback control response for the loop. Note that when $\dot{\omega}_{n,ij}(t) = 0$ (47), (48) reduce to the constant eigenvalues $\lambda_{ij} = -\zeta\omega_n \pm j\omega_n\sqrt{1-\zeta^2}$.

The actuator dynamics are ignored in the controller design as they are viewed as a singular perturbations to the closed-loop system, with a bandwidth much larger than the highest

bandwidth in the closed-loop controller. By the singular perturbation principle, the bandwidth ω_{nij} are initially set to $\omega_{nij} = \frac{1}{3}\omega_{n(i+1)j}$. The bandwidth of the rotational, longitudinal, and lateral dynamics are set respectively to $\omega_{n4,1} < \frac{1}{3}\omega_{n,rd}$, $\omega_{n2,1} < \frac{1}{3}\omega_{n,sh}$, $\omega_{n2,2} < \frac{1}{3}\omega_{n3,1} < \frac{1}{3}\omega_{n,rd}$. Bandwidth tuning of ω_{nij} will be performed from the rotational dynamic loop successively one loop at a time. $F_{y,ctrl}$ is not used in the controller implementation for under-actuated MSVs.

C. Control Allocation

The actuator commands are calculated from the commanded force and torque by nonlinear inversion of the actuator models (11)-(14) as:

$$F_{Cx,com} = F_{Cx,nom} + F_{x,ctrl} \quad (49)$$

$$N_{C,com} = N_{nom} + N_{ctrl} \quad (50)$$

The commanded force $F_{Cx,com}$ and torque $N_{C,com}$ are then used to compute $\omega_{sh,com}$ and $\delta_{rd,com}$:

$$\mathcal{T}_{sh} = F_{Cx,com} + \mathcal{D}_{rd} \quad (51)$$

$$\omega_{sh,com} = \sqrt{\mathcal{T}_{sh}/k_{\mathcal{T}_p}} \quad (52)$$

$$\delta_{rd,com} = \frac{N_{C,com}}{l_x(\mathcal{T}_{sh}(1 + k_{\mathcal{L}_n}\omega_{sh})(k_{\mathcal{L}\delta_1}))} \quad (53)$$

IV. SIMULATION RESULTS

The effectiveness of the proposed MNL-TLC trajectory tracking control algorithm is demonstrated by simulation using a well-known sub-scale MSV model, the CyberShipII [1]. The actuator model is modified to match the underactuation condition of the present work i.e. no lateral thruster is used. There are three types of trajectories, with constant $\bar{u}$, that can be considered, in order of tracking control challenge levels:

1) Straight line: Unaccelerated with constant ψ_{nom} and ramp P_{nom}, and zero β_{nom}.
2) Circle: Unaccelerated with ramp ψ_{nom}, sinusoidal P_{nom}, and constant β_{nom}.
3) Sine wave: accelerated with sinusoidal $v_{nom}, r_{nom}, \psi_{nom}$, and β_{nom}.

In this paper the first test trajectory is not presented. The tuned controller parameters for the other two cases are summarized in the Table I. The MSV model parameters are taken from [1], [27] with adaptation to an equivalent single propeller-rudder configuration. The actuator saturation limits are set to $max(|\delta_{rd}|) = 30^\circ$ and $max(|\omega_{sh}|) = 16\ rad/s$.

A. Test Trajecotry 2

A circular trajectory is used to demonstrate both accelerated tracking in the transient phase and un-accelerated tracking performance in steady state. The radius of the circle is $R = 11\ m$ and the steady state tangential velocity of $V = 0.13\ m/s$. The simulation results are shown in Fig. 8 - Fig. 11. While the cumulative open-loop tracking error appears large, as shown in Fig. 6, its initial errors are sufficiently small so that the feedback control based on the trajectory linearization is exponentially stable and robust. The closed loop response is a clear improvement over the open loop

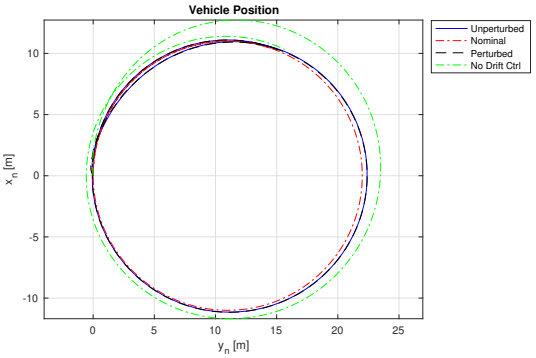

Fig. 8. 2D Trajectory of Closed-loop Control

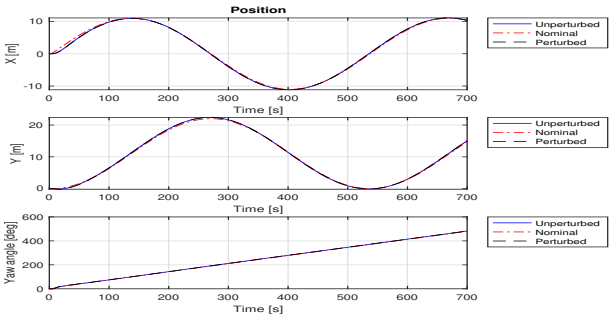

Fig. 9. Position Tracking

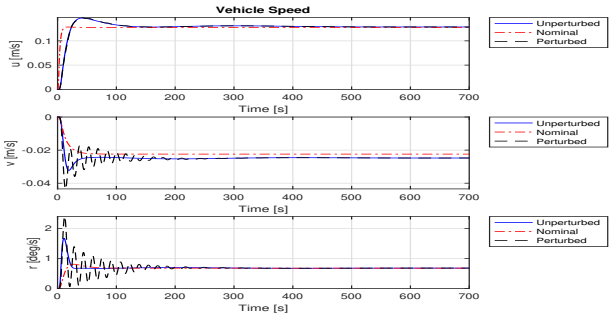

Fig. 10. Velocity Tracking

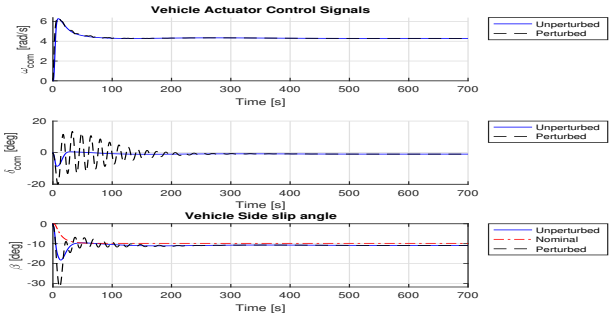

Fig. 11. Actuator Command Signals

control response, with smooth and benign actuator activities. The PI-control law for each of the 4 loops is a Type-I system with zero steady state error for constant inputs. However the kinematics variables have nonzero steady-state errors due to the sinusoidal trajectories. To further reduce these steady-state errors, a Type-II controller can be employed at the cost of reduced agility and stability margins. To exemplify the stability robustness, simultation results for a 6X mismatched I_z for the vehicle model and the controller, which may happen in practice by cargo distribution on a ship, are also shown in Fig. 8 - Fig. 11. The tracking error for unperturbed and perturbed cases are summarized in Table II. It is of particular interest to note that β, in Fig. 11, has a non-negligible rate of change and has a steady-state values around 11°. This demonstrates that the restrictions on β as presented in [9], [10], [15] have been overcome by the proposed MNL-TLC algorithm. Furthermore, Fig. 8 shows that the proposed lateral force generation algorithm yields a clear improvement over the case without it. Where the peak lateral error $||y_{b,err}||_\infty$ is reduced from 1.93 m to 0.42 m, some 3.5X improvement, and the RMS error $||y_{b,err}||_2$ goes from 1.05 m to 0.23 m, an improvement of 3.6X.

B. Test Trajectory 3

A sinusoidal trajectory with amplitude of 12 m and a wavelength of 74 m is used to demonstrate accelerated tracking with variant r_{nom}, v_{nom} and β in both the transient and steady-state tracking performance, which is a more challenging task compared to the steady set point in the generalized velocities v_{nom} and r_{nom} of the circular trajectory. The results are shown in Fig. 12- Fig. 15. A 5X I_z perturbation case is also included.

Tracking error metrics for both circular and sinewave trajectories with and without I_z perturbations are summarized in Table II. It is noted that the I_z perturbations had minimal effects for both trajectories. The allowable perturbation is limited by integrator windup.

V. CONCLUSIONS

An integrated 3DOF trajectory tracking control algorithm based on the MNL-TLC architecture for under-actuated MSVs has been presented, which is considered a complex control challenge in [9], [22]. The challenge of lateral drift when turning is tackled by using the sideslip angle β as a virtual control effector. A new enabling algorithm is presented for determining the nominal sideslip angle β_{nom} based

TABLE I
CONTROLLER PARAMETERS

	Guidance Outer Loop	Guidance Inner Loop	Steering Outer Loop	Steering Inner Loop
Nominal Controller				
ζ	[0.9 0.9]	[1.4 1.4]	1.4	1.4
$\omega_n[rad/s]$	[10 10]	[1/27 1/21]	1/5	1
Feedback Controller				
ζ	[0.9 .0.9]	[1.4 0.7]	1.4	0.9
$\omega_n[rad/s]$	[1/500 1/500]	[1/45 1/75]	1/15	1/3

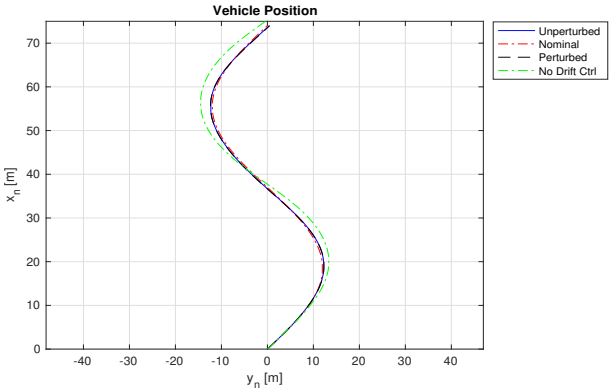

Fig. 12. 2D Trajectory of Closed-loop Control

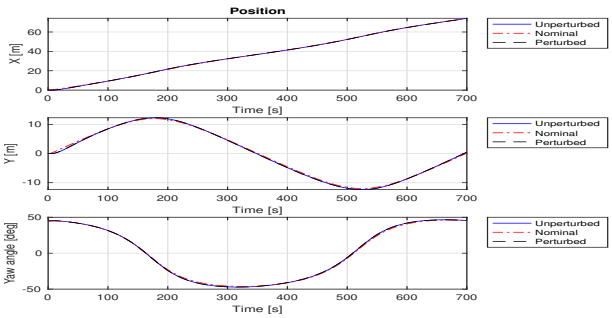

Fig. 13. Position Tracking

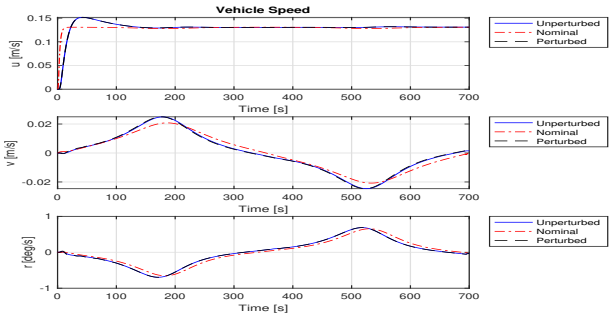

Fig. 14. Velocity Tracking

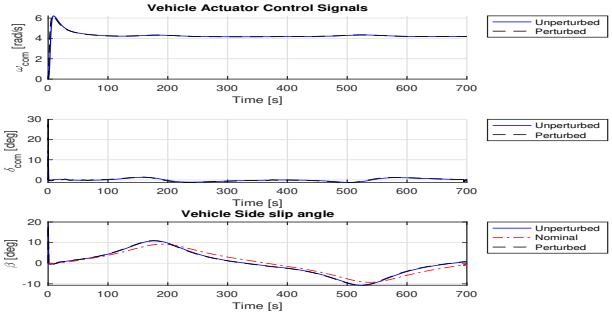

Fig. 15. Actuator Command Signals

TABLE II

TRAJECTORY TRACKING ERRORS

	Error Metric	Circular Traj.		Sine Traj.	
		Unpert.	Pert.	Unpert.	Pert.
$x_{b,err}$ $[m]$	$\|\|*\|\|_\infty$	1.058	1.111	1.041	1.041
	$\|\|*\|\|_2$	0.281	0.297	0.256	0.255
$y_{b,err}$ $[m]$	$\|\|*\|\|_\infty$	0.425	0.415	0.408	0.419
	$\|\|*\|\|_2$	0.228	0.225	0.239	0.257
ψ_{err} $[rad]$	$\|\|*\|\|_\infty$	0.050	0.070	0.025	0.028
	$\|\|*\|\|_2$	0.030	0.031	0.015	0.016
u_{err} $[\frac{m}{s}]$	$\|\|*\|\|_\infty$	0.094	0.094	0.095	0.095
	$\|\|*\|\|_2$	0.011	0.012	0.011	0.011
v_{err} $[\frac{m}{s}]$	$\|\|*\|\|_\infty$	0.016	0.031	0.0045	0.0047
	$\|\|*\|\|_2$	0.003	0.004	0.0024	0.0026
r_{err} $[\frac{rad}{s}]$	$\|\|*\|\|_\infty$	0.022	0.033	0.0019	0.0019
	$\|\|*\|\|_2$	0.002	0.004	0.0011	0.0011

on the reference kinematic pose and the dynamic forces along a nominal trajectory. This approach allows for an under-actuated MSV to track an accelerated trajectory with 3.5X reduction in lateral tracking error under closed-loop control, as demonstrated by simulation with a realistic sub-scale vessel model. Guidelines and demonstrative examples on the tuning of inverse dynamics in the open loop nominal controller have been presented, which provide an insight on the response of the nominal controller and its effects on the overall controller transient response, steady-state tracking errors, and resulting actuator activities. The simulation results for the closed-loop tracking of a circular and a sinewave trajectory, which demonstrate tracking performance of both accelerated and un-accelerated trajectories, are provided as a baseline verification of the proposed algorithm. To exemplify the robustness of the controller, circular and sinusoidal trajectories with 6X and 5X mismatch of the yaw moment of inertia I_z, respectively, in the vehicle and controller are simulated, showing minimal performance degradation. Simulation tests with more challenging trajectories, performance under disturbances, robustness with model mismatch, Type-II controller for the kinematics loops, and optimal controller tuning are subjects of future work.

REFERENCES

[1] R. e. a. Skjetne, "Adaptive maneuvering, with experiments, for a model ship in a marine control laboratory," *Automatica*, vol. 44, pp. 289–298, Feb 2005.

[2] Y. Yang, J. Du, H. Liu, C. Guo, and A. Abraham, "A trajectory tracking robust controller of surface vessels with disturbance uncertainties," *IEEE Transactions on Control Systems Technology*, vol. 22, no. 4, pp. 1511–1518, 2013.

[3] X. Sun and S. S. Ge, "Adaptive neural region tracking control of multi-fully actuated ocean surface vessels," *IEEE/CAA Journal of automatica sinica*, vol. 1, no. 1, pp. 77–83, 2014.

[4] J. Jiao and G. Wang, "Event triggered trajectory tracking control approach for fully actuated surface vessel," *Neurocomputing*, vol. 182, pp. 267–273, 2016.

[5] Z. Zheng, Y. Huang, L. Xie, and B. Zhu, "Adaptive trajectory tracking control of a fully actuated surface vessel with asymmetrically constrained input and output," *IEEE Transactions on Control Systems Technology*, vol. 26, no. 5, pp. 1851–1859, 2017.

[6] Z. Shen, Y. Bi, Y. Wang, and C. Guo, "Mlp neural network-based recursive sliding mode dynamic surface control for trajectory tracking of fully actuated surface vessel subject to unknown dynamics and input saturation," *Neurocomputing*, vol. 377, pp. 103–112, 2020.

[7] F. Del-Rio-Rivera, V. M. Ramírez-Rivera, A. Donaire, and J. Ferguson, "Robust trajectory tracking control for fully actuated marine surface vehicle," *IEEE Access*, vol. 8, pp. 223 897–223 904, 2020.

[8] M. S. Triantafyllou and F. S. Hover, *Maneuvering and control of marine vehicles*. Massachusetts of Institute of Technologyq, 2003.

[9] T. I. Fossen, K. Y. Pettersen, and R. Galeazzi, "Line-of-sight path following for dubins paths with adaptive sideslip compensation of drift forces," *IEEE Transactions on Control Systems Technology*, vol. 23, no. 2, pp. 820–827, 2014.

[10] Y. Yu, C. Guo, and H. Yu, "Finite-time plos-based integral sliding-mode adaptive neural path following for unmanned surface vessels with unknown dynamics and disturbances," *IEEE transactions on automation science and engineering*, vol. 16, no. 4, pp. 1500–1511, 2019.

[11] K. D. Do, "Practical control of underactuated ships," *Ocean Engineering*, vol. 37, no. 13, pp. 1111–1119, 2010.

[12] Y. Liu and J. J. Zhu, "Singular perturbation analysis for trajectory linearization control," in *2007 American control conference*. IEEE, 2007, pp. 3047–3052.

[13] Y. Liu and J. J. Zhu, "Regular perturbation analysis for trajectory linearization control," in *2007 American Control Conference*. IEEE, 2007, pp. 3053–3058.

[14] H. Khalil, "Nonlinear systems," *3rd edition*, 2002.

[15] Y. Wang, Y. Qu, S. Zhao, R. Cajo, and H. Fu, "Smooth sliding mode control for path following of underactuated surface vehicles based on los guidance," *Journal of Marine Science and Engineering*, vol. 11, no. 12, p. 2214, 2023.

[16] B. Qiu, G. Wang, Y. Fan, D. Mu, and X. Sun, "Course controller design for unmanned surface vehicle based on trajectory linearization control with input saturation," *Chinese Control And Decision Conference (CCDC)*, pp. 281–286, June 2019.

[17] D. Mu, G. Wang, Y. Fan, B. Qiu, and X. Sun, "Adaptive course control based on trajectory linearization control for unmanned surface vehicle with unmodeled dynamics and input saturation," *Neurocomputing*, vol. 330, pp. 1–10, Feb 2019.

[18] B. Qiu, G. Wang, and Y. Fan, "Predictor los-based trajectory linearization control for path following of underactuated unmanned surface vehicle with input saturation," *Ocean Engineering*, vol. 214, p. 107874, 2020.

[19] Y. Zhao and J. Jim Zhu, "Automatic aircraft loss-of-control prevention by bandwidth adaptation," *Journal of Guidance, Control, and Dynamics*, vol. 40, no. 4, pp. 878–889, 2017.

[20] Y. Chen, J. Zhu, and L. Lin, "Integrated forward and reverse trajectory tracking control for car-like ground vehicle," *Dynamic Systems and Control Conference*, vol. 59162, p. V003T21A007, Oct 2019.

[21] J.-M. Godhavn, "Nonlinear tracking of underactuated surface vessels," in *Proceedings of 35th IEEE Conference on Decision and Control*, vol. 1. IEEE, 1996, pp. 975–980.

[22] T. Fossen, *Handbook of Marine Craft Hydrodynamics and Motion Control*. Wiley, 2011.

[23] G. Zhang and X. Zhang, "Practical robust neural path following control for underactuated marine vessels with actuators uncertainties," *Asian Journal of Control*, vol. 19, no. 1, pp. 173–187, 2017.

[24] S. He, S. Dai, and F. Luo, "Asymptotic trajectory tracking control with guaranteed transient behavior for msv with uncertain dynamics and external disturbances," *IEEE Transactions on Industrial Electronics*, vol. 66, pp. 3712–3720, Jul 2018.

[25] S. Dai, S. He, M. Wang, and C. Yuan, "Adaptive neural control of underactuated surface vessels with prescribed performance guarantees," *IEEE transactions on neural networks and learning systems*, vol. 30, pp. 3686–3698, Jul 2018.

[26] B. S. Park, J.-W. Kwon, and H. Kim, "Neural network-based output feedback control for reference tracking of underactuated surface vessels," *Automatica*, vol. 77, pp. 353–359, 2017.

[27] K. Lindegaard and T. Fossen, "Fuel-efficient rudder and propeller control allocation for marine craft: Experiments with a model ship," *IEEE Transactions on Control Systems Technology*, vol. 11, pp. 850–862, Nov 2003.

[28] Y. Chen and J. Zhu, "Car-like ground vehicle trajectory tracking by using trajectory linearization control," *ASME 2017 Dynamic Systems and Control Conference. American Society of Mechanical Engineers Digital Collection*, 2017.